STUDY OF THE FLOW-INDUCED VIBRATION OF THE DOWNSTREAM CYLINDER IN A TANDEM ARRANGEMENT

Bruno S. Carmo, bruno.carmo@usp.br
NDF, Department of Mechanical Engineering, Poli, University of São Paulo, Brazil

Spencer J. Sherwin, s.sherwin@imperial.ac.uk
Peter W. Bearman, p.bearman@imperial.ac.uk
Department of Aeronautics, Imperial College London, UK

Richard H. J. Willden, richard.willden@eng.ox.ac.uk
Department of Engineering Science, University of Oxford, UK

Abstract. *Two-dimensional numerical simulations of the flow around two circular cylinders in tandem arrangements are performed. The upstream cylinder is fixed and the downstream cylinder is free to oscillate in the transverse direction, in response to the fluid loads. The Reynolds number is kept constant at 150 and the reduced velocity is varied by changing the structural stiffness. The in-line centre-to-centre distance is varied from 1.5 to 8.0 diameters, and the results are compared to that of a single isolated cylinder mounted on an elastic base with the same structural characteristics. The calculations show that significant changes occur in the dynamic behaviour of the cylinders, when comparing the flow around the tandem arrangements to that around an isolated cylinder: for the tandem arrangements, the lock-in boundaries are wider, the maximum displacement amplitudes are greater and the amplitudes of vibration for high reduced velocities, outside the lock-in, are very significant. The main responsible for these changes appears to be the oscillatory flow in the gap between the cylinders.*

Keywords: *flow-induced vibration, circular cylinder, wake interference, numerical simulation*

1. INTRODUCTION

The flow around circular cylinders has been extensively studied due to its practical importance in engineering and scientific relevance in fluid mechanics. When circular cylinders are grouped in close proximity, the flow field and the forces experienced by the cylinders can be entirely different from those observed when the bodies are isolated in the fluid stream. The effect of the presence of other bodies in the flow is called *flow interference*. One of the most severe types of interference, and the type on which this paper focuses, is *wake interference*, which happens when the cylinder is immersed or in close proximity to the wake of another bluff body. In such situations, the flow impinging on the cylinder is usually totally different from the free stream. Given the number of differences observed in the forces exerted on cylinders subjected to wake interference when compared to the single cylinder case, one expects that the flow-induced vibrations (FIV) experienced by a flexible cylinder or a compliantly-mounted rigid cylinder will also be different depending whether the cylinder is immersed in a vortex wake or not.

A few papers on this matter have been published, most of them were concerned with vibrations within the synchronisation range, i.e. when the vortex shedding is synchronised with the cylinder vibration. King and Johns (1976) investigated the vibration of two flexible cylinders in tandem by performing experiments in a water channel. Bokaian and Geoola (1984) carried out experiments on the flow around circular cylinders in tandem and staggered arrangements, the upstream cylinder being fixed and the downstream one being rigid and mounted on an elastic base that allowed cross-stream displacement. Zdravkovich (1985) investigated the behaviour of two flexible circular cylinders placed in diverse arrangements using a wind tunnel. Brika and Laneville (1999) utilised wind tunnel experiments to study the flow induced vibrations of a flexible circular cylinder, allowed to vibrate in one plane only, immersed in the wake of a rigid cylinder. Assi et al. (2006) performed experiments on the FIV of a elastically-mounted rigid cylinder in the wake of a fixed identical cylinder, using a water channel. Recently, there has also been a few computational studies on FIV of two circular cylinders in tandem. Examples of this type of work are Mittal and Kumar (2001), Jester and Kallinderis (2004) and Papaioannou et al. (2008). In all these papers, the computations were two-dimensional and focused on reduced velocities within the synchronisation range. In general terms, they confirmed the main conclusions of previously published experimental data: the wake interference led to a wider synchronisation range and within this range the amplitude of response was larger than that observed in the response of an isolated cylinder with the same structural parameters.

However, some papers have also reported that cylinders subjected to wake interference also experienced vibrations with high amplitudes for higher reduced velocities, outside the synchronisation range (Bokaian and Geoola, 1984; Zdravkovich, 1985; Brika and Laneville, 1999; Hover and Triantafyllou, 2001). In most cases, the amplitude levels were even higher than those observed in the lock-in. Although the reduced velocity for which this peculiar type of response starts to be significant seems to depend on various aspects, such as the separation between the cylinders and the

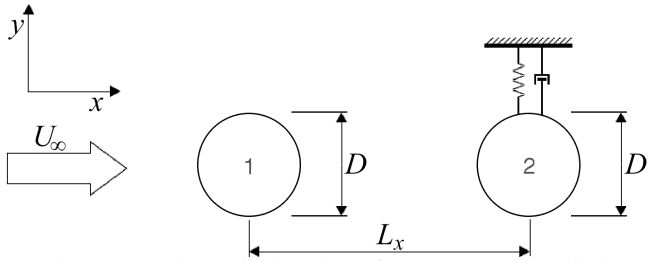

Figure 1: Schematic drawing of arrangement studied.

mass ratio, all the papers agree on the fact that an upper reduced velocity limit for which these vibrations would cease does not seem to exist.

As we can see, the number of publications on flows around circular cylinders affected by wakes of other circular cylinders is not small. However, the parameter space to be investigated in such flows is considerably larger than in the flow around an isolated cylinder. For instance, we can vary the streamwise and cross-stream separations between the bodies, the orientation of the axis of the cylinders, the number of cylinders and the ratio between the diameters of the cylinders. Furthermore, in the case of FIV, we can also consider some cylinders fixed and others allowed to oscillate in one or two directions, in addition to using different structural parameters for each cylinder. Because of this large number of parameters to be analysed, the basic understanding about flows with wake interference is far from being comparable to the knowledge on the flow around an isolated cylinder. This paper aims at decreasing this gap.

An often used approach to tackling problems with such a large parameter space is to model the phenomenon based on a deep understanding of its physics, obtained by the investigation of one or a few simple cases where the phenomenon is present. If the model is sufficiently consistent with the physics, its extrapolation to a number of other similar cases is likely to be valid. Therefore, to understand how the approaching wake interacts with a compliant body, we investigated the flow around a circular cylinder mounted on an elastic basis, allowed to move only in the transverse direction, immersed in the wake of an upstream fixed circular cylinder of the same diameter D placed at a streamwise centre-to-centre distance L_x, as sketched in figure 1. This is a very useful model to study wake interference, since the number of parameters is kept to a reasonable quantity for a proper systematic analysis so the basics of the interference mechanisms can be more easily understood. Although we also present results for reduced velocities in the synchronisation range, we focus particularly on the high reduced velocity response of the downstream cylinder, employing two-dimensional numerical simulations.

2. NUMERICAL METHOD

The fluid-structure interaction problem this paper of interest comprises the flow around two bodies, with one of them being allowed to move independently of the other. The computational code used to simulate the flow therefore uses an Arbitrary Lagrangian-Eulerian (ALE) formulation was employed. The ALE formulation allows one to incorporate arbitrary displacements of the mesh into the governing equations, so the movement of the bodies and the mesh deformations necessary to maintain an adequate spatial discretisation can be taken into account.

The ALE form of the incompressible Navier-Stokes equations involve a simple modification in the advection term of the usual form of the Navier-Stokes equations. The resulting equations, written in non-dimensional form are

$$\frac{\partial \mathbf{u}}{\partial t} = -(\mathbf{u} - \mathbf{m}) \cdot \nabla \mathbf{u} - \nabla p + \frac{1}{Re} \nabla^2 \mathbf{u}, \tag{1}$$

$$\nabla \cdot \mathbf{u} = 0. \tag{2}$$

The cylinder diameter D is the reference length and the free-stream speed U_∞ is the reference speed used in the non-dimensionalisation. $\mathbf{u} \equiv (u, v, w)$ is the velocity field, $\mathbf{m}$ is the velocity of the coordinate systems attached to the mesh, also referred to as velocity of the mesh, t is the time, p is the modified static pressure, i.e. divided by the constant density ρ, $Re = \rho U_\infty D/\mu$ is the Reynolds number and μ is the dynamic viscosity of the fluid. The numerical solution of these equations was calculated using a Spectral/*hp* discretisation as described in Karniadakis and Sherwin (2005).

In the FIV problems considered in this paper, we assumed that the moving cylinder was rigid and mounted on an elastic base that allows displacement in only one direction; such behaviour of an oscillating structure is described by the equation of a linear mass-spring-damper system forced by the fluid load. This equation can be written in non-dimensional form as

$$M^* \ddot{y}_c^* + C^* \dot{y}_c^* + K^* y_c^* = F_y^*(\ddot{y}_c^*, \dot{y}_c^*, y_c^*, t^*), \tag{3}$$

where M^* is the non-dimensional mass of the oscillating system, C^* is the non-dimensional structural damping coefficient, K^* the non-dimensional stiffness coefficient and F_y^* is the non-dimensional force imposed by the fluid in the

direction of motion. These non-dimensional parameters are related to their dimensional counterparts M, C, K and F_y by the expressions

$$M^* = \frac{M}{\rho D^2 L}, \qquad C^* = \frac{C}{\rho U_\infty D L}, \qquad K^* = \frac{K}{\rho U_\infty^2 L}, \qquad F_y^* = \frac{C_L}{2} = \frac{F_y}{\rho U_\infty^2 D L},$$

where L is the (axial) length of the cylinder and C_L is the lift coefficient. The variables $\ddot{y}_c^*$, $\dot{y}_c^*$, y_c^* are the non-dimensional acceleration, velocity and displacement of the body, respectively, and t^* is the non-dimensional time. These variables are non-dimensionalised according to the expressions

$$\ddot{y}_c^* = \frac{\ddot{y}_c D}{U_\infty^2}, \qquad \dot{y}_c^* = \frac{\dot{y}_c}{U_\infty}, \qquad y_c^* = \frac{y_c}{D}, \qquad t^* = \frac{t U_\infty}{D}.$$

This non-dimensionalisation scheme was adopted in order to make the non-dimensional form of the structure and flow equations consistent, so the coupling between the structure and flow solvers could be more easily undertaken. However, M^*, C^* and K^* are not the most common choice of non-dimensional parameters in the literature. For ease of comparison with previously published data, the results of this paper are presented as a function of the mass ratio, m^*, damping ratio, ζ, and reduced velocity, V_r. These non-dimensional parameters are defined as

$$m^* \equiv \frac{4M}{\rho \pi D^2 L}, \qquad \zeta \equiv \frac{C}{2\sqrt{KM}}, \qquad V_r \equiv \frac{U_\infty}{f_n D}.$$

where f_n is the natural frequency of the structure in a vacuum ($f_n = \sqrt{K/M}/(2\pi)$).

The equations (1), (2) and (3) have to be solved in a coupled manner. The fluid load F_y^* in eq. (3) is calculated from the solution of the flow equations (1)-(2), and the motion of the boundaries, which are necessary for the solution of eqs. (1)-(2), is determined by the solution of the structure equation (3). In this work, the structure and flow solvers were loosely coupled, similar to the work of in Jester and Kallinderis (2004), since the time step sizes necessary for the solution of the flow equations (i.e. the CFL restriction) were sufficiently small to yield convergent loosely-coupled schemes. The structure equation (3) was integrated using Newmark's scheme (Newmark, 1959), the mesh deformation was calculated using the spring mesh model proposed by Batina (1990) and the mesh movement was incorporated to the time splitting scheme of the flow solver in a similar fashion as in Beskok and Warburton (2001).

3. RESULTS

The configurations tested had separations $L_x/D = 1.5$, 3, 5 and 8. These configurations were chosen because of the different shedding regimes they present for fixed arrangements (for a classification of shedding regimes, see for example Zdravkovich, 1987; Carmo et al., 2010). In addition, simulations of the flow around a single cylinder mounted on an elastic base with the same structural parameters were performed, to serve as a benchmark. The number of elements of the meshes employed varied from 507 to 811 depending on the configuration, and Jacobi polynomials of degree 8 were used in the expansion base. The boundaries of the meshes were located $36D$ upstream from the upstream cylinder, $45D$ downstream from the downstream cylinder and $50D$ from the centres of the cylinders in the cross-stream direction on both sides. The size of the mesh and level of discretisation were based on the convergence studies in Carmo (2005). Uniform stream velocity boundary conditions ($u = 1$, $v = 0$) were imposed at the upstream and side boundaries of the computational domain. At the cylinder walls, a no-slip condition was imposed so the fluid had the same velocity as the body, and at the downstream boundary Neumann conditions, $\partial u/\partial \mathbf{n}$=0, $\partial v/\partial \mathbf{n} = 0$ were applied.

The mass ratio and structural damping of the elastic base were $m^* = 2.0$ and $\zeta = 0.007$, chosen to match the structural parameters of the experiments carried out by Assi et al. (2008). The reduced velocities tested ranged from 3.0 to 30.0, varied by changing the spring stiffness and keeping the Reynolds number constant at 150. The non-dimensional time step was 0.006. All FIV simulations were started from fully-developed flows obtained from two-dimensional simulations with the cylinders fixed and $Re = 150$.

3.1 Single cylinder

The results obtained for the flow around a single cylinder (figure 2) show the typical response of vortex-induced vibrations at low Reynolds numbers and low mass ratio (see figure 12 in Williamson and Govardhan, 2004). There is a very well defined lock-in range, where the vortex shedding frequency locks to a value close to the natural frequency of the structure, as can be seen in the frequency plot in figure 2. The lock-in range can be divided into an initial and a lower branch. The initial branch covers the range $3.0 \leq V_r \leq 5.5$, and has a phase angle ϕ close to 0°. It is in the initial branch that the amplitude reaches its highest value for the reduced velocities investigated, $A/D = 0.582$. For $5.5 < V_r < 6.0$ the phase angle changes abruptly from a value close to 0° to a value close to 180°, and this marks the transition between the initial and lower branches. The lower branch extends from $V_r \approx 6.0$ to $V_r \approx 7.5$, and for this range the cylinder exhibits

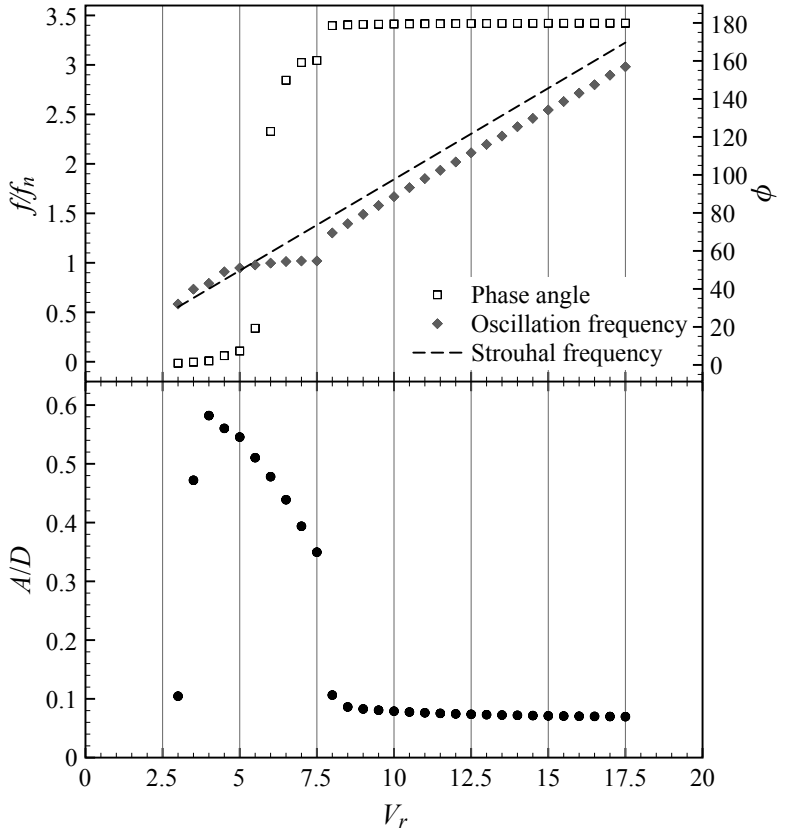

Figure 2: Non-dimensional amplitude (A/D), phase angle (ϕ) and frequency plots against reduced velocity for the flow around an isolated cylinder, $Re = 150$, two-dimensional simulations. The Strouhal frequency is the vortex shedding frequency in the flow around a fixed cylinder at the same Reynolds number.

fairly large amplitudes of vibration ($0.3 < A/D < 0.5$). For reduced velocities higher than those of the lower branch ($V_r \geq 8.0$) the amplitude of vibration is low ($A/D < 0.1$), and the phase angle is close to $180°$.

The shedding pattern for the whole range of reduced velocities investigated was 2S. However, there is a striking difference between the wakes in the initial and lower branches, as can be seen in figure 3. When the response is at the initial branch (figure 3(a)), the resulting wake is wide, with the vortices forming two parallel rows further downstream. In contrast, the wake of the lower branch is narrow and similar to that observed for a fixed cylinder, with the vortices alternating in a line parallel to the free stream (figure 3(b)). This difference in the wakes is consistent with the different phase angles of the branches.

3.2 Tandem arrangements – small separations

The structural responses in the two-dimensional simulations for the configurations $L_x/D = 1.5$ and $L_x/D = 3.0$ were very similar; figure 4 shows the results for $L_x/D = 3.0$. The synchronisation range starts at $V_r \approx 4.0$; this reduced velocity is higher than that for which the synchronisation range starts for the single cylinder ($V_r \approx 3.0$, see figure 2). This can be explained by the fact that the mean flow in the wake is slower than the free stream. Like the isolated cylinder, the lock-in region for the tandem arrangements with small separations can be divided into an initial and a lower branch. The initial branch covers $4.0 \leq V_r \leq 6.0$, and exhibits the highest amplitudes of the entire response range. The peak amplitude was observed for $V_r = 6.0$ and its value was slightly higher than $0.9D$, which is more than 50% larger than the peak amplitude observed for the isolated cylinder. As the reduced velocity is increased, the initial branch is followed by a lower branch, where the amplitude of vibration decreases smoothly, instead of showing the abrupt decrease observed for the single cylinder case. For the tandem arrangements, the range for which the downstream cylinder vibrates with significant amplitudes does not have an upper V_r limit like in the single cylinder case. For reduced velocities from 15 up to 30, the amplitude of vibration is surprisingly high (between $0.4D$ and $0.5D$), and the phase angle is close to $180°$. In this same velocity range, the isolated cylinder vibrated with negligible amplitudes ($A/D < 0.1$).

Regarding the frequency of vibration, also shown in figure 4, it can be seen that for the first few points the frequencies follow the Strouhal line, but they stop coinciding as soon as the amplitude of vibration becomes large. For $4.5 \leq V_r \leq 8.0$, the frequency of vibration is close to the natural frequency of the structure, but the data points show an almost parallel trend to the Strouhal frequency, different from the flat plateau observed for the single cylinder case in the lock-in region.

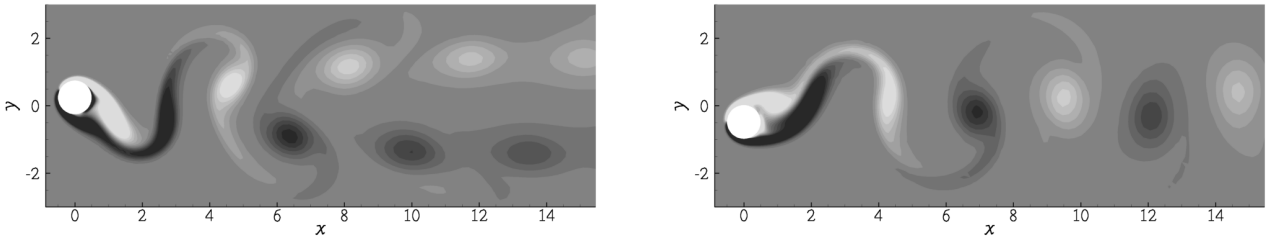

(a) $V_r = 5.0$ – initial branch (b) $V_r = 6.0$ – lower branch

Figure 3: Instantaneous vorticity contours illustrating the wake at the initial and lower branches. Light (dark) shades of grey correspond to negative (positive) vorticity. Isolated cylinder, $Re = 150$, two-dimensional simulations.

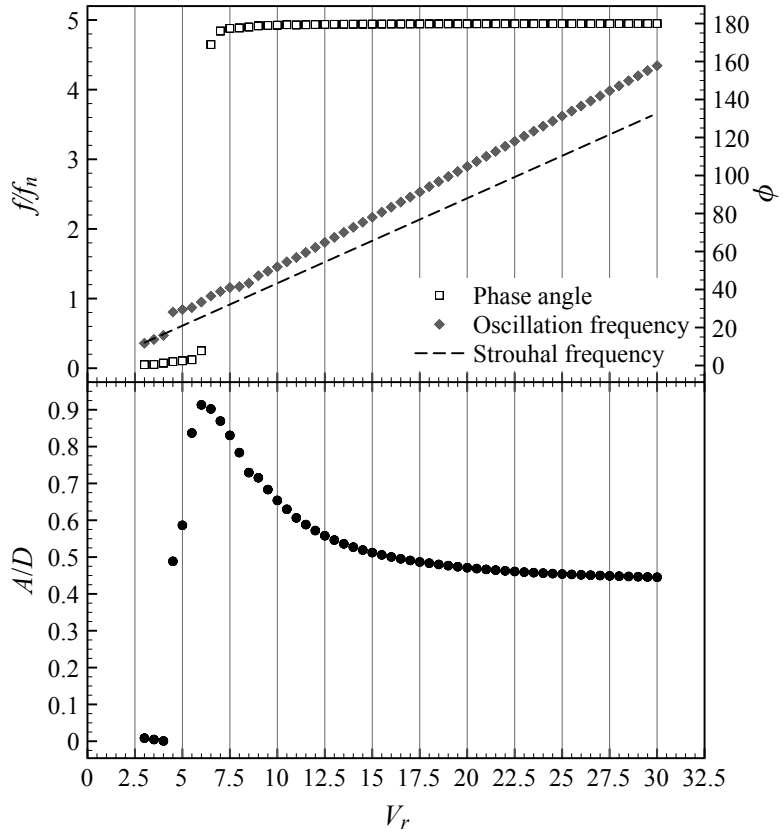

Figure 4: Amplitude, phase angle and frequency plots against reduced velocity for the downstream cylinder in a tandem arrangement with $L_x/D = 3$, $Re = 150$, two-dimensional simulations.

It is also in this reduced velocity range, more specifically for $6.0 < V_r < 6.5$, that the phase angle jump occurs. For $V_r > 8.5$ the frequency of vibration follows a linear trend with positive slope; however this slope is different from that of the Strouhal line for the fixed arrangement. The reason for this can be identified by looking at the vorticity contours in figure 5. Once the downstream cylinder starts to vibrate with a reasonable amplitude, the shedding regime changes from that of when the cylinder is fixed, and so does the main frequency of shedding and consequently the frequency of oscillation.

It should be noted that when the downstream cylinder is vibrating with high amplitudes, the vortices roll up upstream of the leeward cylinder, but they are still connected to the upstream cylinder through the shear layer when they impinge on the downstream cylinder. The complete detachment of the vortex from the upstream body happens only as the downstream cylinder moves across the wake, cutting off the shear layer, as illustrated by the sequence of three contour plots in figure 6. Consequently, for configurations with small separations the motion of the downstream cylinder is tightly coupled with the vortex shedding from the upstream cylinder. The normalised power spectral density (PSD) contours of the displacement and upstream lift coefficient signals shown in figure 7 show that the spectra of these signals are practically the same. An important conclusion from this observation is that in the lock-in range, the shedding from the upstream cylinder is also synchronised with the motion of the downstream cylinder.

Like the single cylinder in the lock-in range, the force that drives the cylinder immediately after an extreme of displacement originates from the vortex being formed at the side of the cylinder closer to the wake centreline, as can be seen

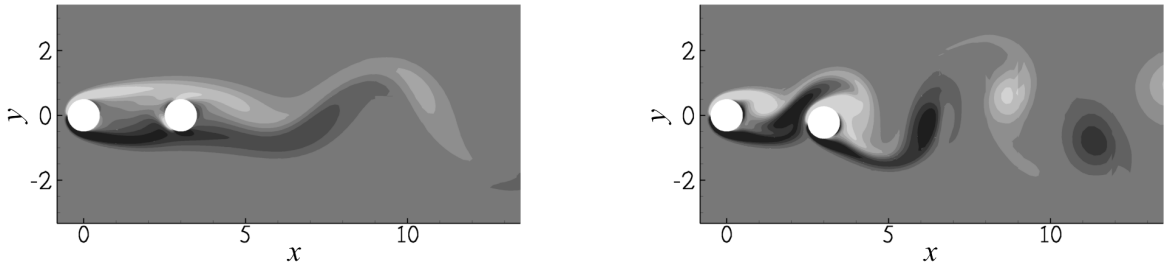

(a) Fixed cylinders (b) $V_r = 10.0$

Figure 5: Instantaneous vorticity contours illustrating different shedding regimes. $L_x/D = 3$, $Re = 150$, two-dimensional simulations.

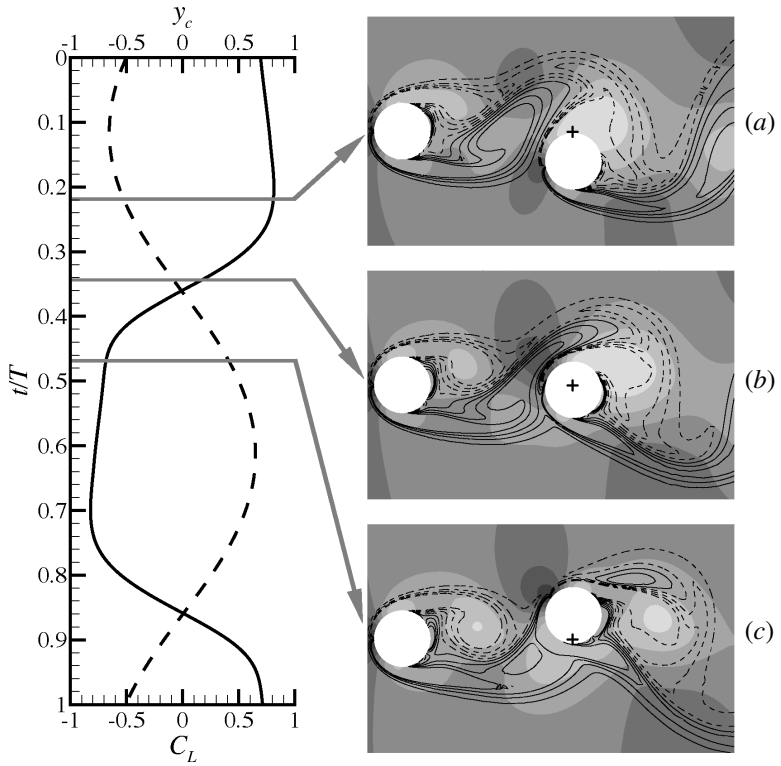

Figure 6: *Left* – Graph of the lift coefficient (solid) and cylinder displacement (dashed) over one cycle. *Right* – vorticity iso-lines superposed on pressure contours at selected instants of the oscillation cycle. Continuous lines represent positive vorticity and dashed lines represent negative vorticity. Dark grey contours represent high pressures and light grey contours represent low pressures. The cross indicates the neutral position of the cylinder. The arrows indicate the moment of the cycle each of the flow fields refers to. Two-dimensional flow around two cylinders in tandem with $L_x/D = 3$, $V_r = 10.0$, $Re = 150$.

in figure 6(a). Also similarly to the single cylinder at synchronisation, the force that mostly contributes to the cylinder deceleration when the body is approaching an extreme of displacement is the high pressure of the stagnation point shifted to the outer part of the wake, as illustrated in figure 6(c). The difference is that for the tandem arrangement, the shifting of the front stagnation point does not depend exclusively on the motion of the cylinder, but is decisively influenced by the oscillatory flow upstream. Figure 8 shows instantaneous streamtraces of the field pictured in figure 6(c). It can be seen that the streamtraces approaching the downstream cylinder are curved towards the wake centreline due to the velocity induced by the vortex in the near wake of the upstream cylinder.

3.3 Tandem arrangements – large separations

For the largest separations investigated, $L_x/D = 5$ and $L_x/D = 8$, the structural response differed from what was observed for the isolated cylinder and for the tandem arrangements with smaller separations. The results for $L_x/D = 5$ and $L_x/D = 8$ exhibited the same behaviour; shown in figure 9 are the results for $L_x/D = 8$. The first difference from the smaller separations data is the presence of an easily identified lock-in region: for $5.0 \lesssim V_r \lesssim 15.0$ the cylinder

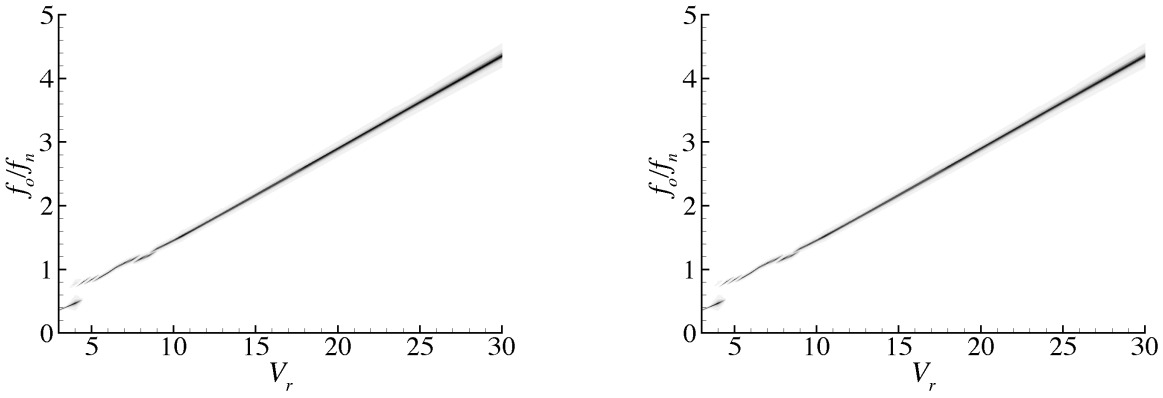

(a) Downstream cylinder y_c (b) Upstream cylinder C_L

Figure 7: Contours of normalised power spectral density of the cylinder displacement signal, as a function of the reduced velocity. $L_x/D = 3$, $Re = 150$, two-dimensional simulations.

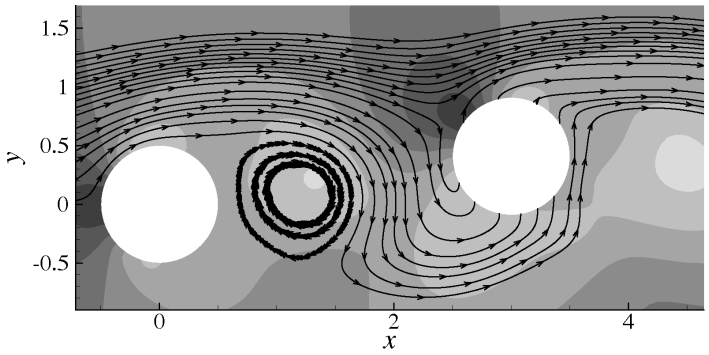

Figure 8: Instantaneous streamtraces superposed on pressure contours. Dark (light) contours correspond to high (low) pressures. Two-dimensional flow around two cylinders in tandem with $L_x/D = 3$, $V_r = 10.0$, $Re = 150$.

vibrates at a frequency close to the structural natural frequency, instead of following the Strouhal frequency. In this range, the shedding from the downstream cylinder has a strong component at the natural frequency of the structure. It is worth highlighting that the synchronisation range is much wider for $L_x/D = 8$ and $L_x/D = 5$ than for the single cylinder case. Another evident feature of the large separation arrangements' lock-in region is a secondary peak in the amplitude, appearing where the Strouhal frequency is approximately equal to $1.5f_n$. At the higher end of the synchronisation region, the amplitude of vibration levels out smoothly to a value which is significantly higher than that observed for the single cylinder case, but lower than those observed for the small separations. This large vibration appears to be sustained indefinitely for high reduced velocities.

In figure 9 only the frequency with the highest energy is plotted. However, there are important components of the force spectrum at other frequencies. The PSD contours of the displacement signal shown in figure 10(a) reveal how the secondary peaks in the spectrum vary with the reduced velocity. The peaks at the higher frequencies, which follow a straight line of positive slope, correspond to the shedding from the upstream cylinder. This can be verified by comparing this curve with that in figure 10(b), which shows the PSD of the upstream cylinder lift coefficient signal. The peaks at the lower frequencies in figure 10(a) do not have the same origin for the entire range of reduced velocities. Within the lock-in range ($5.0 \lesssim V_r \lesssim 15.0$), these peaks are at frequencies close to the natural frequency of the structure, as expected. It is interesting to notice that the vibration of the downstream cylinder does not affect the shedding of the upstream cylinder. This is an important difference between the responses of the downstream cylinder in tandem arrangements with small and large separations, since the results for small separations in section 3.3showed that in the lock-in range, the shedding from the upstream cylinder was synchronised with the downstream cylinder oscillation.

For reduced velocities higher than those of the lock-in, figure 10(a) shows that the lower frequency peaks follow another straight line of positive slope. The frequencies on this line are approximately half of the frequency of the upstream cylinder shedding at the same reduced velocity. These peaks originate from the interaction between the vortices in the wake of the downstream cylinder, which gives rise to the secondary wake observed for tandem and staggered arrangements with streamwise separation larger than the drag inversion spacing. As reported in Carmo et al. (2008), the secondary wake has a dominant frequency equal to half the frequency of vortex shedding. It seems that the formation of the secondary wake has a strong influence on the forces and consequently the response of the downstream cylinder, since it can delay or anticipate the shedding of the vortices. Like the arrangements with smaller separations, the two main mechanisms

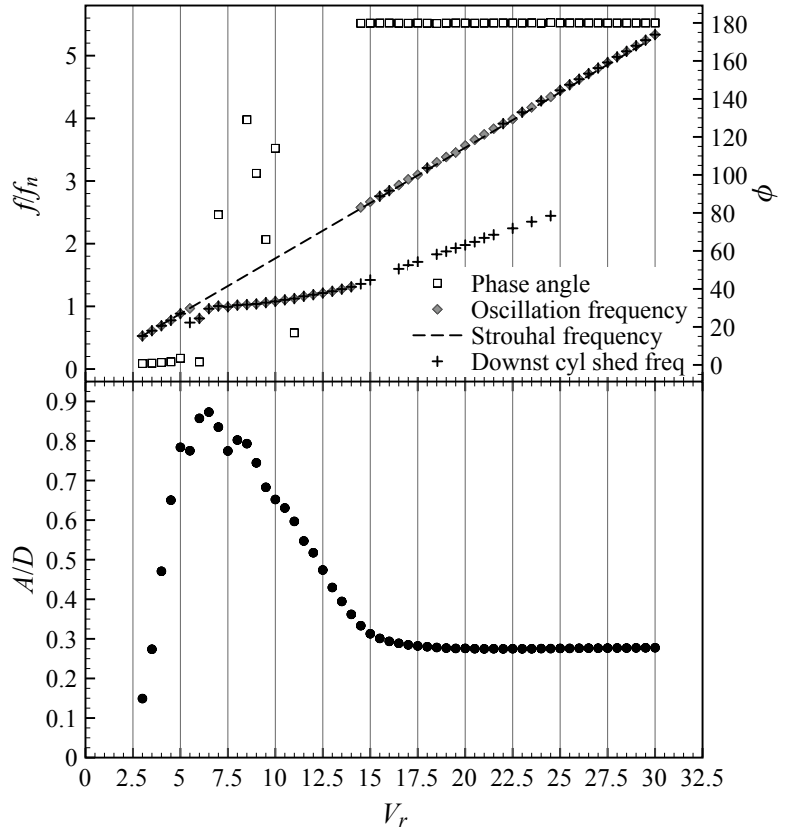

Figure 9: Amplitude, phase angle and frequency plots against reduced velocity for the for the downstream cylinder in a tandem arrangement with $L_x/D = 8$, $Re = 150$, two-dimensional simulations.

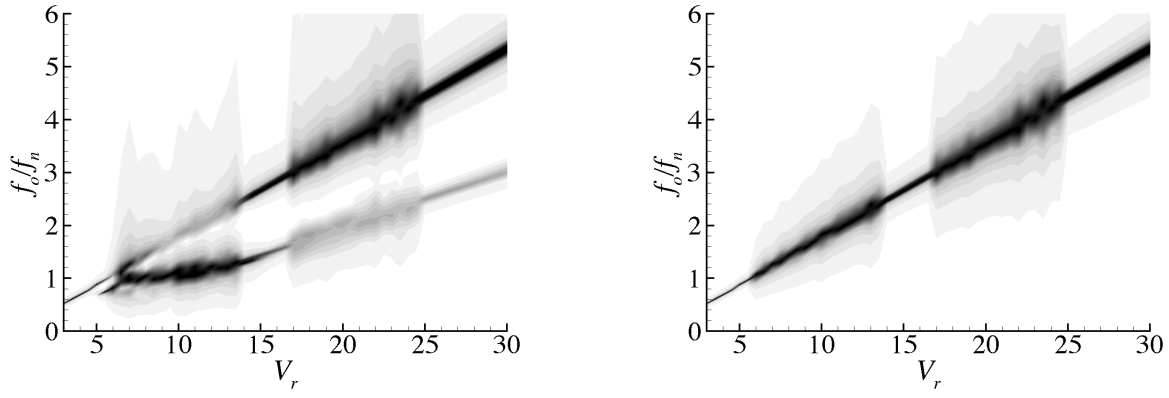

(a) Downstream cylinder y_c (b) Upstream cylinder C_L

Figure 10: Contours of normalised power spectral density of the cylinder displacement signal, as a function of the reduced velocity. $L_x/D = 8$, $Re = 150$, two-dimensional simulations.

responsible for the excitation of the cylinder are the lower pressure regions generated by the vortices being shed and the shifting of the high pressure region at the front stagnation point.

The fact that the shedding from the upstream cylinder shows a rather clean spectrum (figure 10(b)) suggests that this irregular character of the response has its origins in the wake downstream of the leeward cylinder. When the forces are in phase with the displacement, the cylinder experiences its higher amplitudes of vibration; the shear layers separating from the leeward cylinder interact and the wake formed downstream is regular, as illustrated in figure 11(a). However, this state is not sustained when the amplitudes get too large, the phase angle shifts to a value close to 180° and the amplitude decreases gradually, until one of the vortices from the upstream cylinder impinges on the downstream cylinder at a phase which puts the force again in-phase with the displacement, and the amplitude builds-up again. This behaviour is repeated with some regularity, but is not totally periodic.

For reduced velocities close to the second peak, figure 11(b) shows that the shear layers in the near wake of the downstream cylinder do not interact as for the previous case ($V_r = 6.5$), and the far wake is very irregular. For higher

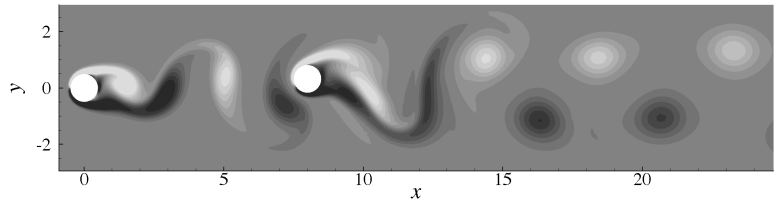

(a) $V_r = 6.5$

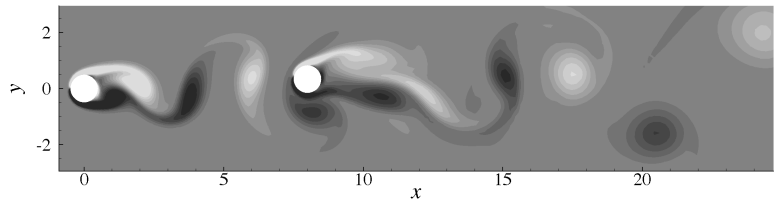

(b) $V_r = 8.5$

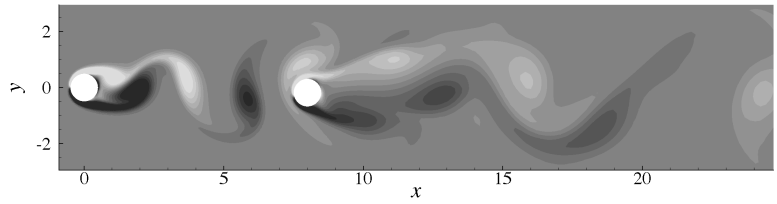

(c) $V_r = 20.0$

Figure 11: Instantaneous vorticity contours for diverse reduced velocities, $L_x/D = 8$, $Re = 150$, two-dimensional simulations.

reduced velocities, the phase angle is consistently at values close to $180°$, and the wake downstream is wide and irregular (figure 11(c)).

4. CONCLUSIONS

We have employed direct numerical simulations to analyse the structural response and flow fields obtained for tandem arrangements with diverse centre-to-centre separations, the upstream cylinder being fixed and the downstream cylinder being free to oscillate in the transverse direction. The Reynolds number was kept constant at $Re = 150$ while the reduced velocity was varied by changing the structural stiffness.

The results showed that there are significant changes in the structural response of the downstream cylinder in the tandem arrangements when compared to an elastically mounted single cylinder. The lock-in region boundaries are modified: it is difficult to define an upper limit for configurations with small separations ($L_x/D \leq 3$) and for larger cylinder separations, the lock-in region is much wider than in the single cylinder case. The maximum displacement amplitude observed in the synchronisation range is also larger, approaching values 50% higher than the maximum displacement amplitude of the single cylinder case. In addition, the displacement amplitude responses at high reduced velocities were very significant, in some cases comparable to the highest amplitude in the single cylinder case. The physical mechanism responsible for these differences appears to be related to the oscillatory flow in the gap between the cylinders, which causes the front stagnation point of the downstream cylinder to shift alternatively along the upstream portion of the cylinder wall.

Although many insights were gained from the FIV results reported in this paper, there is still a number of issues that remain to be investigated. One of them is the dependence of the response on the Reynolds number, and this question is already being addressed by the authors. Other topics that are worth investigating are the FIV of cylinders allowed to move in the streamwise as well as the cross-stream direction, the FIV in arrangements where the upstream cylinder is also compliantly-mounted, the development of reduced models to predict the response of the cylinders and the design of effective FIV suppressors for flows with wake interference.

ACKNOWLEDGEMENTS

The authors would like to thank Gustavo Assi for the enlightening discussions about this work. B.S.C. acknowledges the support from Capes / MEC - Brazil during his PhD at Imperial College London.

5. REFERENCES

Assi, G. R. S., Bearman, P. W., Meneghini, J. R., 2008. Unsteady response of a circular cylinder under wake-induced excitation from a fixed upstream cylinder. In: Zoloratev, I., Horáček, J. (Eds.), Flow-Induced Vibration 2008. Prague, Czech Republic.

Assi, G. R. S., Meneghini, J. R., Aranha, J. A. P., Bearman, P. W., Casaprima, E., 2006. Experimental investigation of flow-induced vibration interference between two circular cylinders. Journal of Fluids and Structures 22, 819–827.

Batina, J. T., August 1990. Unsteady euler airfoil solutions using unstructured dynamic meshes. AIAA Journal 28 (8), 1381–1388.

Beskok, A., Warburton, T. C., 2001. An unstructured hp finite-element scheme for fluid flow and heat transfer in moving domains. Journal of Computational Physics 174, 492–509.

Bokaian, A., Geoola, F., 1984. Wake-induced galloping of two interfering circular cylinders. Journal of Fluid Mechanics 146, 383–415.

Brika, D., Laneville, A., 1999. The flow interaction between a stationary cylinder and a downstream flexible cylinder. Journal of Fluids and Structures 13, 579–606.

Carmo, B. S., 2005. Numerical investigation of the flow around two cylinders in tandem arrangements. MSc dissertation, Escola Politécnica - University of São Paulo, Brazil.

Carmo, B. S., Meneghini, J. R., Sherwin, S. J., 2010. Secondary instabilities in the flow around two circular cylinders in tandem. Journal of Fluid Mechanics 644, 395–431.

Carmo, B. S., Sherwin, S. J., Bearman, P., Willden, R., 2008. Wake transition in the flow around two circular cylinders in staggered arrangements. Journal of Fluid Mechanics 597, 1–29.

Hover, F. S., Triantafyllou, M. S., 2001. Galloping response of a cylinder with upstream wake interference. Journal of Fluids and Structures 15, 503–512.

Jester, W., Kallinderis, Y., 2004. Numerical study of incompressible flow about transversely oscillating cylinder pairs. Journal of Offshore Mechanics and Arctic Engineering - Transactions of the ASME 126, 310–317.

Karniadakis, G. E., Sherwin, S. J., 2005. Spectral/hp Element Methods for Computational Fluid Dynamics, 2nd Edition. Oxford University Press, Oxford-UK.

King, R., Johns, D. J., 1976. Wake interaction experiments with two flexible circular cylinders in flowing water. Journal of Sound and Vibration 45 (2), 259–283.

Mittal, S., Kumar, V., 2001. Flow-induced oscillations of two cylinders in tandem and staggered arrangements. Journal of Fluids and Structures 15, 717–736.

Newmark, N. M., 1959. A method of computation for structural dynamics. Journal of the Engineering Mechanics Division of ASCE 85, 67–94.

Papaioannou, G. V., Yue, D. K. P., Triantafyllou, M. S., Karniadakis, G. E., AUG 2008. On the effect of spacing on the vortex-induced vibrations of two tandem cylinders. Journal of Fluids and Structures 24 (6), 833–854.

Williamson, C. H. K., Govardhan, R., 2004. Vortex-induced vibrations. Annual Review of Fluid Mechanics 36 (413-455).

Zdravkovich, M. M., 1985. Flow-induced oscillations of two interfering circular cylinders. Journal of Sound and Vibration 101 (4), 511–521.

Zdravkovich, M. M., 1987. The effects of interference between circular cylinders in cross flow. Journal of Fluids and Structures 1 (2), 239–261.

Responsibility notice

The author(s) is (are) the only responsible for the printed material included in this paper